Experimental study on the lateral cyclic response of the piles in sand

Javad Keshavarz[1], Jafar Bolouri Bazaz[2*]

1. PhD student of Geotechnical Engineering, Ferdowsi University of Mashhad, Mashhad, Iran

Email: keshavarz@mail.um.ac.ir, Tel.:

2. Associate Professor, Civil Engineering Department, Ferdowsi University of Mashhad, Mashhad, Iran

Email: bolouri@um.ac.ir, Tel.:

Abstract

The established foundation type for most offshore wind turbines is monopile. Due to waves and wind, the monopile of such structures experiences cyclic loading that causes the rearrangement of the soil grains around the pile, altering the damping ratio and stiffness of the soil-pile system. In this study, the impact of changing the loading frequency and soil density on the horizontal displacement, stiffness, and damping ratio on piles under cyclic lateral load has been evaluated. A series of experimental tests have been carried out by applying one-way cyclic lateral loading with three frequencies on PVC piles with different length-to-diameter (L/B) ratios in loose and dense sand. The horizontal displacement, stiffness, and damping ratio values were obtained for each test. Also, the constant coefficients of equations proposed by other researchers (to determine deformation, stiffness, and damping ratios) were evaluated. The results are presented that the change of loading frequency has a considerable influence on the absolute values of displacement, stiffness, and damping ratio, however, it has a negligible effect on constant coefficients.

Keywords: Cyclic lateral loading, Loading frequency, Stiffness, Damping ratio

1. Introduction

Vast developments have been made during the last decades in offshore wind turbines, fulfilling an essential role in reducing carbon dioxide levels [1]. These types of structures are

commonly established on single monopole piles [2]. The cyclic loads applied to the foundation of offshore structures are principally caused by wind and waves. The number of cyclic loads is usually more than one million during their lifetime. The responses of these structures can be categorized into four types: elastic, elastic shakedown, plastic shakedown, and ratcheting behavior [3].

Soil–pile system degradation occurs during cyclic loading, consisting of 'material' and 'mechanical' degradation [4]. Material degradation is the consequence of changes in soil properties like density and pore pressure. In contrast, mechanical degradation results from soil yield occurring along the pile or by gaps developing between the soil and pile [5]. Figure 1 depicts the three states of soil behavior subject to cyclic loading concluded from experimental and numerical research, including progressive failure, stabilization, and shakedown [6, 7].

Insert Figure 1

The shakedown state develops during accumulated plastic strains, decreasing with the number of cycles, leading to material stabilization (i.e., only elastic deformation occurs) [8]. The cyclic load applied to the pile may be one- or two-way, symmetrical or asymmetrical, and induced by load-controlled or displacement-controlled modes [9].

It is well known that the cyclic lateral load on the pile leads to an accumulation of permanent displacements with the number of load cycles [10-13]. The rate of permanent accumulation deformations tends to diminish with the number of cycles [14]. The secant stiffness is usually greater than the initial stiffness and grows with each cycle [15]. Figure 2 depicts the two types of stiffness defined in the literature: absolute (ka) and cyclic (kc) secant stiffness [16].

Insert Figure 2

Some researchers have reported that monopile cyclic secant stiffness increases with the number of cycles [11, 17-19]. Furthermore, the cyclic stiffness dramatically increases in the first few cycles [20], so that 90% of the growth is acquired in the first 20 cycles [21]. However, a decrease in cyclic stiffness has been observed under specific cyclic loadings [22-24]. The cyclic stiffness of the system largely depends on the magnitude and characteristics of the applied cyclic displacement [25].

The influence of frequency on dry sand seems to be negligible when the range of loading frequency is less than 1 Hz [16]. According to the drained cyclic simple shear test with a frequency below 1.9 Hz, no dependence was observed between the rate of accumulated

displacement and frequency [26]. Also, this phenomenon was reported due to the effect of the load frequency on the residual strains in the drained cyclic triaxial test on ballast with a loading frequency between 0.1 and 30 Hz [27]. In contrast, some researchers showed that the behavior of soil tends to become stiffer at higher loading rates, [28] i.e., the pile head displacement increases with an increase in frequency (0.45, 0.65, and 0.94 Hz) for the same number of cycles [29].

In general, the damping of the foundation-structure system is entirely dependent on the structural vibrations [30]. The damping of wind turbine structures involves the combination of hydrodynamic damping, aerodynamic damping, tower oscillation dampers, structural damping, and soil damping [31], among which soil damping is most influential yet cannot be easily estimated [30].

Soil damping falls into three categories: radiation damping, material damping, and pore-pressure dissipation. Although elastic wave propagation generates radiation damping within soil mass with a relatively high load frequency ($f > 1Hz$), the damping of material is affected by the soil hysteretic phenomenon, corresponding to the dissipation of energy by the soil. Finally, damping results from pore-pressure dissipation if the pile is installed in coarse materials with high permeability [32, 33].

The published research cited herein focused mainly on the deformation behavior of piles under cyclic lateral loading, yet comprehensive studies have not been dedicated to the influence of frequency variations on the soil properties. This research gap encouraged the authors to investigate the response of piles under cyclic lateral load. In this study, a cyclic test program has been arranged to evaluate the impact of changing the loading frequency and soil density on the horizontal displacement, stiffness, and damping ratio.

2. Materials

2.1 Soil

Offshore wind turbines are installed in a wide range of soil conditions and various layers, ranging from dense sands to stiff clays, rocks, and layered soils. For example, the soil layers in the typical marine strata of the North Sea consist of sandy and coarse media [34]. This paper focuses on the response of piles in granular materials [19, 35].

The soil used in this investigation was Firoozkooh sand, with its grain size distribution being depicted in Figure 3. Table 1 represents other soil specifications, classifying it as poorly graded sand (SP).

Insert Figure 3

Insert Table 1

2.2 Pile

PVC pipes with embedded lengths of 400, 600, and 800 mm were used as the piles. A variety of length to diameter ratios (*L/B*) were adopted to cover the behavior of both short and long piles based on the relative stiffness of the soil–pile system. The mechanical specifications of the PVC pipe are summarized in Table 2.

Insert Table 2

3. Experimental setup

3.1 Sample preparation

A new raining system designed and developed at the Soil Mechanics Research Center of Ferdowi University, was employed to fill the reservoir tank. This system, which has been fully described in detail elsewhere [36], can create a sand bed with a specified density.

3.2 Test setup and loading system

Figure 4 depicts the schematic diagram of the test setup, including loading systems, the soil tank, the data logger, and the terminal box. The soil tank had a rectangular shape with 1200 mm in length, 600 mm in width, and 1000 mm in height. To minimize the boundary effects, the size of the soil tank was taken equal to 8B–12B and 3B-4B in the direction of the lateral load application and perpendicular to this direction [37].

The loading system comprised a servo motor, ball screw, rail, wagon, support bearing, and a load cell with 2 N accuracy placed between the rod and pile (Figure 4). The load eccentricity was kept constant at the height of 350 mm (e=5.5B) relative to the soil surface. This eccentricity fell between approximately 2B and 25B, which some researchers recommend for offshore structures subjected to wind and wave loads [38].

Two series of instruments were employed to measure pile deformation. As the first series, three linear variable differential transformers (LVDTs) were installed at different levels, including the soil surface, the point of load application, and 10 cm beneath this point. These

LVDTs measured the horizontal displacement of the pile. As the second series, eight mechanical gauges were installed outside of the reservoir tank at the depths of 200 mm, 400 mm, 600 mm, and 800 mm (Figure 4). These gauges, which were connected to the pile by flexible wires, were passed through the holes created on the soil tank. They were used to specify the behavior of the pile as flexible or rigid.

Once the tank was filled, the electrical gauge and loading system were positioned on the soil surface and connected to the pile to measure the surface lateral displacement. The raining system was utilized to prepare the soil samples with two relative densities of 24% and 97%, corresponding to the unit weights of 13.8 and 15 kN/m^3, respectively (see Table 3).

Insert Table 3

3.3 Test program and procedure

In the present study, the ultimate static capacity of a pile under horizontal load was derived from the load-displacement curve when the pile head movement reached 0.1B. In this manner, ultimate capacities were assessed for all piles (monotonic tests in Table 4). The one-way cyclic loading (ξ_c =0) tests were conducted while keeping the cyclic load ratio constant (ξ_b=0.4) for different soil densities and different embedded lengths of piles. The non-dimensional parameters, ξ_b and ξ_c, were defined as follows [11]:

ξ_b = (Maximum load)/ (Ultimate static capacity)

ξ_c = (Minimum load)/ (Maximum load)

The number of loading cycles was 5000 with three different frequencies (0.07, 0.14, and 0.28 Hz) for all experiments. The loading frequencies adopted in this research were in the range of 0.05–0.3 Hz, which typically occur during the lifetime of offshore structures [6]. It is worth mentioning that the frequency of cyclic loading of soils is classified between 0 to 1 Hz [39]. The range of typical loads and excitations of an offshore wind turbine is between 0 to 0.5 Hz [40]. Corresponding to the frequency of offshore waves, Abadie set the loading frequency in an experimental investigation at 0.106 Hz [41]. The cyclic load ratio (ξ_b=0.4) has been kept constant, therefore, the maximum load in each cycle is constant. The amplitude in each cyclic test is the maximum load (H_{max}). Amplitudes of cyclic lateral loads have been presented in Table 4.

Each experiment was assigned a unique code as L*f*H or L*f*L. The letter L and f, followed by a number, represent the embedded length (in cm) and loading frequency (in Hz),

respectively. The letters H and L at the end of the number indicate the soil density as high (97%) or low (24%) (Table 3). For example, L60f0.07H indicates that the embedded length of the test pile, loading frequency, and soil density (D_r) were 600 mm, 0.07 Hz, and 97%, respectively. The details of the performed experiments are presented in Table 4.

Insert Figure 4

Insert Table 4

4. Scale effects

Small-scale pile models are preferred in the laboratory because full-scale models are not always feasible due to the high cost and time consumption. Alternatively, small-scale experiments can suffer from scaling effects which should be minimized to ensure that the observed behavior can be extrapolated to predict the full-scale behavior. In this manner all test results have been expressed in non-dimensional form, as shown in Table 5, to enhance the applicability in practice [11].

Insert Table 5

Progressive failure in test models is related to the grain size [42], and it is often recommended that the pile model diameter (B) to particle size (d_{50}) ratio should be above 40 [43]. This ratio was about 90 for the soil used in the current study, indicating the effect of this scale on the experimental results would be negligible. In other investigations, length to diameter ratios of 4, 5, 7, 10, 18, 20, 28, 30, and 38 were used with scaling factors of 1:14, 1:26, 1:30, 1:40, 1:40, 1:50, 1:80, and 1:100 [11, 16, 35, 44, 45]. In the present study, L/B ratios between 6 to 13 and the scaling factor of 1:60 was selected for simulating a single pile in the practical situation with different lengths of 24, 36, and 48 m and a diameter of 3.8 m.

Cuéllar (2011) [16] has employed the scaling rules for all physical quantities as summarized in Table 6 [16, 46].

. Insert Table 6

Based on Table 6, the main dimensions of the study for the prototype and the laboratory model have been shown in Table 7.

Insert Table 7

5. Results and discussion

5.1. Accumulated displacement

Figures 5–7 represent the test results of the pile subjected to the cyclic lateral loading with the embedded lengths of 400 mm, 600 mm, and 800 mm at different load frequencies and soil densities. The pile's horizontal displacement comprises the pile and soil deformation around the pile, which consists of elastic and plastic displacement from a loading cycle. The tests demonstrated that in a specific cyclic loading number (*N*), the higher loading frequency resulted in more pile head displacement than the lower loading frequency. Also, the rate of increasing pile displacement under cyclic loading was more in dense sand than loose sand. The piles with the embedded lengths of 600 mm in loose and dense sand behaved as rigid and flexible piles, respectively.

Insert Figure 5

Insert Figure 6

Insert Figure 7

The pile head horizontal displacement under cyclic lateral loading can be predicted by the following approaches: logarithmic and power functions [47, 48].

$$\frac{y_n}{y_1} = 1 + b\ln(N) \qquad (1)$$

$$\frac{y_n}{y_1} = N^a \qquad (2)$$

In this case, y_1 and y_n are the first and N^{th} lateral displacements under load cycles. Also, *b* and *a* are the constant parameters of the logarithmic and power models. Tables 8 and 9 summarize the magnitudes of *b* and *a*, which depend on many factors such as the soil density, installation method, cyclic load ratio, pile/soil stiffness ratio, and load characteristics [49-55].

Insert Table 8

Insert Table 9

Based on the experimental results of the pile head accumulated displacement, both logarithmic and power models (see Equations 1 and 2) were employed to fit the measured displacement. The values of b and a determined in this manner for all tests and their results are gathered in Table 10. As an example, this approach was adapted for a pile with 600 mm length, embedded in the dense sand (Figures 8).

Insert Figure 8

Insert Table 10

The magnitudes of b and a for flexible and rigid piles with different lengths, soil densities, and load frequencies were in the range of 0.03 to 0.2 and 0.03 to 0.12, respectively (see Table 11). The results show good agreement with other researchers' findings for these parameters (Tables 8 and 9).

Insert Table 11

5.2 Stiffness

It is well known that the stiffness of the soil-pile interaction depends on the number of load cycles. It is represented as follows [56]:

$$(k_{aN} / k_{a1}) = N^{-t} \qquad (3)$$

where k_1 and k_N are the absolute cycle secant stiffness values corresponding to the first and N^{th} cycles, respectively, and t is a constant parameter equal to a for rigid piles as defined in Equation 2 [10]. The test results under one-way horizontal cyclic loading with up to 5000 cycles persuade us to recommend $t=a$ for all types of piles with different conditions.

The dimensionless stiffness is defined for the soil–pile system by Equation 4:

$$\hat{k} = \frac{k}{B\sqrt{\gamma' L P_R}} \qquad (4)$$

where P_R, L, γ', and B are reference stress, embedment length, soil density, and pile diameter, respectively. This equation can be employed for cyclic stiffness evaluation (Equation 4).

The non-dimensional unloading stiffness ($\hat{k}_{uN}$) of the model piles under one-way horizontal cyclic loading is defined in Figure 9, and it can approximately be estimated as follows [11]:

$$\hat{k}_{uN} = \hat{k}_{u1} + A_H \ln(N) \qquad (5)$$

where $\hat{k}_{u1}$ and A_H are the dimensionless unloading stiffness at the first cycle and a constant coefficient, respectively.

Insert Figure 9

The value of A_H was computed by gathering all test results, after which Equation 5 was fitted into the data (see Figure 10-13). Table 12 summarizes the magnitudes of A_H and the coefficient of determination (R^2). Based on experimental research, Leblanc et al. concluded that AH is independent of load characteristics and relative density [11]. However, some researchers (e.g., Chen et al.) believe that this parameter is highly dependent on the relative density of soil. Also they showed there is no apparent correlation with the cyclic ratio [44]. Our test results revealed that the constant A_H is a function of pile length, soil density, and load frequency in both stiff and flexible piles. The data of Table 12 are classified in Table 13 according to different load frequencies and densities. The variations of A_H in different load frequencies and densities are dependent on the soil compaction, resulting from the sand particle subsidence around the pile.

Insert Figure 10

Insert Figure 11

Insert Figure 12

Insert Figure 13

Insert Table 12

Insert Table 13

5.3 Damping ratio

It is well known the evolution of hysteresis loop can be explained by the loop area, which is directly proportional to the soil damping ratio. This issue is presented in the non-dimensional form and represented as follows [41]:

$$\tilde{A}_{hys} = \frac{A_{hys}}{B}\sqrt{\frac{P_R}{L^7 \gamma'^3}} \quad (6)$$

Figure 14 displays the typical pile response to one-way continuous long-term cyclic loading. In the following section, selected cycles are shown to emphasize the evolution of the hysteresis loop shape and pile accumulated deformation with the number of cycles. The test results depicted in Figures 15 to 22 clearly indicate the loop shape tightening with an increasing number of cycles, which follows an exponential decay pattern:

$$\tilde{A}_{N\,(hys)} = \tilde{A}_r N^{-m_A} \quad (7)$$

where $\tilde{A}_r$ is a dimensionless function of the load magnitude and m_A is a power coefficient [41]. To estimate parameter m_A, the variations of the normalized hysteresis area were plotted in terms of the number of cycles for each test, and Equation 7 was fitted to the test data. This procedure, which was employed for all tests, is depicted in Figure 23 for loose sand. Table 14 summarizes the values of m_A, indicating an average m_A value of 0.29.

Insert Figure 14

Insert Figure 15

Insert Figure 16

Insert Figure 17

Insert Figure 18

Insert Figure 19

Insert Figure 20

Insert Figure 21

Insert Figure 22

Insert Figure 23

The pile subjected to cyclic horizontal loading undergoes two phases of densification and convection. The densification phase starts from the first loading cycle, and a rearrangement among soil particles occurs due to lateral pile displacement, leading to soil compaction. It is well known that densification generally leads to the soil stiffening around the pile, which may

produce significant variations in the cyclic behavior of the foundation in the long term [57]. This behavior, which depends on the soil and pile conditions, results in the shakedown and ratcheting states [3]. The second phase commences when the soil reaches the maximum possible density. During this phase, a ratcheting deformation occurs in the soil particles based on the cyclic lateral movements of the pile (see Figure 24) [16, 58]. It is important to emphasize that both convective grain migration and densification take place simultaneously.

According to the tests depicted in Figures 15 to 22, the pile reaches the ratcheting displacement in loose sand more quickly than the dense one.

Insert Figure 24

The damping ratio as a non-dimensional parameter is generally employed to measure dissipation of energy. This parameter is specified as the ratio between the energy which has been dissipated during one cycle over the total elastic energy, i.e.[58]

$$D_a = \frac{1}{4\pi}\frac{A_{hys}}{A_{el}} \qquad (8)$$

where A_{hys} is the dissipated energy or sum of the energy consumed due to both hysteretic and ratcheting behavior, approximated by the loop area. In Figure 25, the area enclosed by the reload-unload loop is shown as highlights within the gray surface. Accordingly, A_{el} is the stored elastic energy, which is defined by the upper triangle from the mean load to the maximum load amplitude (hatched area, Figure 25) [59].

The cyclic damping ratio can be calculated as follows [41]:

$$D_{aN} = D_{a0}N^{-m_d} \qquad (9)$$

where D_{a0} is the first loop damping ratio, and m_d is a constant coefficient estimated by experimental tests. The damping ratio calculated for each of our tests and for loose sand is depicted in Figure 26 in terms of the number of cycles. It is possible to estimate m_d by fitting Equation 9 to the damping ratio calculated in Equation 8. The magnitudes of m_d are summarized in Table 14. Also, the range of D_{a0} reported in Table 15 is comparable with the results of other investigations. For instance, Abadie *et al*. estimated the first cycle damping ratio as 0.28, and Byrne evaluated this parameter in the value of 0.2 based on laboratory tests [41, 60].

Insert Figure 25

Insert Figure 26

Insert Table 14

Insert Table 15

6. Design Recommendation

Although a great number of parametric studies on experimental and full-scale piles should be conducted to provide an applicable design methodology, the research represented herein suggests employing the logarithmic and power functions to determine pile head displacement after N loading cycles. The range of the constant coefficient in the functions is roughly 0.03 to 0.2, and the value of the first damping ratio is between 0.15 and 0.45. The absolute secant stiffness reduces with the load cycles. However, the cyclic secant stiffness may increase or decrease with the number of cycles, largely depending on the magnitude and characteristics of the applied cyclic loading and soil density.

7. Limitations

One of the primary limitations of the study presented in this paper is related to the limited soil conditions. This research evaluated the response of piles in sandy soil, which according to the many sites of monopile foundation may be located in clay or limestone in the field [61]. The experiments were performed on dry sand and it was anticipated that the results would be similar due to the reduction of water pressure in the saturated sand quickly [62].

The tests have been conducted at 1 g condition which may affect soil dilatancy and friction angle in comparison with the field [11, 44]. finally, the characteristics of wave and wind load in the field are very complicated but in this research, the loading pattern was regular [16].

8. Conclusion

This paper focuses on the behavior of monopiles subjected to cyclic lateral loading embedded in dry loose and dense sands with loading frequency variations in the range of 0 to 0.3 Hz. Based on the test result, the proposed equations for displacement, unloading stiffness, and damping ratio by other researchers were calibrated and the constant coefficients were determined. As the main findings, it is shown that the loading frequency variations have a considerable effect on the absolute values of displacement, unloading stiffness, and damping

ratio but an insignificant effect on the constant coefficients of equations. Also, the other conclusions can be summarized as follows:

- An increase in either the number of cycles or frequency leads to an increment in the lateral displacement of a single pile under one-way cyclic horizontal loading.

- There is generally a high degradation of the hysteresis loop area and damping ratio in the first ten cycles, reaching less than half of the initial magnitude.

- The hysteresis loop area reduces by increasing the number of cycles. Consequently, the loop area changes to resemble a line shape, indicating elastic behavior (ratcheting displacement); this occurs more quickly in loose sand than dense sand.

- Both logarithmic and power function models properly predicted the accumulated displacements using constant parameters of "*a*" and "*b*". The magnitudes of "*b*" and "*a*" for dense and loose sand were in the range of 0.03 to 0.2 and 0.03 to 0.12, respectively. These values were specified based on different embedded pile lengths at three loading frequencies and depend on the soil conditions, type of piles, and loading conditions.

- The non-dimensional unloading stiffness of the soil-pile system subjected to lateral loading increases with the number of load cycles. However, the absolute secant stiffness decreases with the load cycles. The magnitude of coefficient A_H (Equation 5) in unloading stiffness depends on soil density, embedded length pile, and load frequency.

Declaration of Competing Interest

The authors declare that they have no known competing financial interests or personal relationships that could influence the work reported in this paper.

List of notations

a = constant parameter of power equation;
A_{el} = area corresponding to elastic energy;
A_H = constant coefficient in unloading stiffness equation;
A_{hys} = hysteresis loop area;
$\tilde{A}_{hys}$ = normalized hysteresis area;
b = constant parameter of logarithmic equation;
B = outer diameter of the pile;
C_c = curvature coefficient;
k_a = absolute secant stiffness;
k_c = cyclic secant stiffness
$\hat{k}$ = non-dimensional stiffness;
$\hat{k}_{uN}$ = non-dimensional unloading stiffness;
L = embedded length of the pile;
m_A = power coefficient in hysteresis area equation;
m_d = constant coefficient in damping ratio equation;
n = scaling factor;

C_u = uniformity coefficient;

d_{50} = average grain size;

D_a = damping ratio;

D_r = relative density of the soil;

e = load eccentricity;

EI = stiffness of the pile;

E_s = Young's modulus of the soil;

f = load frequency;

G_s = specific gravity;

H = lateral load;

H_{max} = maximum amplitudes of lateral load;

$\overline{H}$ = normalized lateral load;

N = number of cycles;

P_R = reference pressure;

t = constant parameter in absolute secant stiffness equation;

u = horizontal displacement in unloading stiffness;

y = pile head lateral displacement;

$\acute{\gamma}$ = effective unit weight of soil;

γ_s = unit weight of soil;

φ = friction angle for the sand;

ξ_b, ξ_c = load characteristic parameters;

λ = aspect ratio;

δ = displacement ratio;

References

1. Bai, Y. Li, D.-y. and Zhang, Y.-k. "Accumulated Rotation of A Modified Suction Caisson and Soil Deformation Induced by Cyclic Loading", *China Ocean Engineering*. **34**, pp. 441-449 (2020).
2. Ding, Z. Song, C. Chen, L., et al. "Dynamic analysis of laterally loaded single piles in sandy soils considering sliding and debonding on the pile-soil interface", *Ocean Engineering*. **217**, pp. 107720 (2020).
3. Collins, I. and Boulbibane, M. "Geomechanical analysis of unbound pavements based on shakedown theory", *Journal of Geotechnical and Geoenvironmental Engineering*. **126**(1), pp. 50-59 (2000).
4. Swane, I.C. "The cyclic behaviour of laterally loaded piles," University of Sydney, (1983).
5. Heidari, M. El Naggar, H. Jahanandish, M., et al. "Generalized cyclic p–y curve modeling for analysis of laterally loaded piles", *Soil Dynamics and Earthquake Engineering*. **63**, pp. 138-149 (2014).
6. Lesny, K. and Hinz, P. "Design of monopile foundations for offshore wind energy converters", *in Contemporary topics in deep foundations* pp. 512-519.(2009).
7. Lesny, K. and Hinz, P. "Investigation of monopile behaviour under cyclic lateral loading", *in Offshore site investigation and geotechnics, confronting new challenges and sharing knowledge*. Society of Underwater Technology (2007).
8. Rasmussen, K.L. Hansen, M. Wolf, T.K., et al. "A literature study on the effects of cyclic lateral loading of monopiles in cohesionless soils", *Department of Civil Engineering, Aalborg University, DCE Technical Memorandum*. (25) (2013).
9. Basack, S. "Design recommendations for pile subjected to cyclic load", *Marine Georesources & Geotechnology*. **33**(4), pp. 356-360 (2015).
10. Albiker, J. Achmus, M. Frick, D., et al. "1 g model tests on the displacement accumulation of large-diameter piles under cyclic lateral loading", *Geotechnical Testing Journal*. **40**(2), pp. 173-184 (2017).
11. LeBlanc, C. Houlsby, G. and Byrne, B. "Response of stiff piles in sand to long-term cyclic lateral loading", *Géotechnique*. **60**(2), pp. 79-90 (2010).

12. Chong, S.-H. Shin, H.-S. and Cho, G.-C. "Numerical analysis of offshore monopile during repetitive lateral loading", *Geomechanics and Engineering*. **19**(1), pp. 79-91 (2019).
13. Vahabkashi, P. and Rahai, A. "Pile head displacements with different cross sectional shapes under lateral loading and unloading in granular soils", *Scientia Iranica*. **22**(3), pp. 629-638 (2015).
14. Wang, T. Yu, S.-w. Liu, W.-l., et al. "Cyclic Bearing Mechanism of Suction Caissons Supporting Offshore Wind Turbines in Clay", *China Ocean Engineering*. **35**(1), pp. 135-144 (2021).
15. Achmus, M. Thieken, K. Saathoff, J.-E., et al. "Un-and reloading stiffness of monopile foundations in sand", *Applied Ocean Research*. **84**, pp. 62-73 (2019).
16. Cuéllar, P. "Pile Foundations for Offshore Wind Turbines: Numerical and Experimental Investigations on the Behaviour under Short Term and Long-Term Cyclic Loading," PhD, Berlin, Berlin, Germany, (2011).
17. Vicent, S. and Kim, S.-R. "Effects of long-term cyclic horizontal loading on bucket foundations in saturated loose sand", *Applied Ocean Research*. **91**, pp. 101910 (2019).
18. Faresghoshooni, A. Imam, S. and Mahmoodi, A. "Model Testing on the Effects of Section Geometry and Stiffness on the Cyclic Lateral Behavior of Piles in Loose Sand", *International Journal of Civil Engineering*. **19**(5), pp. 563-581 (2021).
19. Tasiopoulou, P. Chaloulos, Y. Gerolymos, N., et al. "Cyclic lateral response of OWT bucket foundations in sand: 3D coupled effective stress analysis with Ta-Ger model", *Soils and Foundations*. **61**(2), pp. 371-385 (2021).
20. Li, Z. Haigh, S. and Bolton, M. "Centrifuge modelling of mono-pile under cyclic lateral loads", *Physical Modelling in Geotechnics*. **2**, pp. 965-970 (2010).
21. EA, A. "Experimental Modelling of Lateral Loads on Large Diameter Mono-Pile Foundations in Sand," PhD, Civil Engineering, Delft University of Technology, Delft, the Netherland, (2011).
22. Liao, W. Zhang, J. Wu, J., et al. "Response of flexible monopile in marine clay under cyclic lateral load", *Ocean Engineering*. **147**, pp. 89-106 (2018).
23. Zhu, N. Cui, L. Liu, J., et al. "Discrete element simulation on the behavior of open-ended pipe pile under cyclic lateral loading", *Soil Dynamics and Earthquake Engineering*. **144**, pp. 106646 (2021).
24. Serras, D.N. Panagaki, S.D. Skalomenos, K.A., et al. "Inelastic lateral and seismic behaviour of concrete-filled steel tubular pile foundations", *Soil Dynamics and Earthquake Engineering*. **143**, pp. 106657 (2021).
25. Darvishi Alamouti, S. Moradi, M. and Bahaari, M.R. "Centrifuge modelling of monopiles subjected to lateral loading", *scientiairanica*. **26**(6), pp. 3109-3124 (2019).
26. Youd, T.L. "Compaction of sands by repeated shear straining", *Journal of Soil Mechanics & Foundations Div*. **98**(sm7) (1972).
27. Kokusho, T. Hara, T. and Hiraoka, R. "Undrained shear strength of granular soils with different particle gradations", *Journal of Geotechnical and Geoenvironmental Engineering*. **130**(6), pp. 621-629 (2004).
28. Kagawa, T. "Cyclic and loading-rate effects on pile responses", *in 3rd International Conference on Numerical Methods in Offshore Piling*. (1986).
29. Basack, S. and Nimbalkar, S. "Measured and predicted response of pile groups in soft clay subjected to cyclic lateral loading", *International Journal of Geomechanics*. **18**(7), pp. 04018073 (2018).
30. Lloyd, G. and Hamburg, G. *Guideline for the certification of offshore wind turbines*. (2005).

31. Devriendt, C. Magalhães, F. El Kafafy, M., et al. "Long-term dynamic monitoring of an offshore wind turbine", *in Topics in Dynamics of Civil Structures, Volume 4Springer* pp. 253-267.(2013).
32. Liang, F. Chen, H. and Jia, Y. "Quasi-static py hysteresis loop for cyclic lateral response of pile foundations in offshore platforms", *Ocean Engineering*. **148**, pp. 62-74 (2018).
33. Zhang, Y. Aamodt, K.K. and Kaynia, A.M. "Hysteretic damping model for laterally loaded piles", *Marine Structures*. **76**, pp. 102896 (2021).
34. Lesny, K. and Wiemann, J. "Design aspects of monopiles in German offshore wind farms", *in Proceedings of the International Symposium on Frontiers in Offshore Geotechnics*. AA Balkema Publishing (2005).
35. Awad-Allah, M.F. Yasufuku, N. and Abdel-Rahman, A.H. "Cyclic response of wind turbine on piles in unsaturated sand", *International Journal of Physical Modelling in Geotechnics*. **17**(3), pp. 161-176 (2016).
36. Abdollahi, M. and Bolouri Bazaz, J. "Reconstitution of sand specimens using a rainer system", *International Journal of Engineering*. **30**(10), pp. 1451-1463 (2017).
37. Rao, S.N. Ramakrishna, V. and Rao, M.B. "Influence of rigidity on laterally loaded pile groups in marine clay", *Journal of Geotechnical and Geoenvironmental Engineering*. **124**(6), pp. 542-549 (1998).
38. Klinkvort, R.T. and Hededal, O. "Lateral response of monopile supporting an offshore wind turbine", *Proceedings of the Institution of Civil Engineers-Geotechnical Engineering*. **166**(2), pp. 147-158 (2013).
39. Peralta, P.a.A., M. "An experimental investigation of piles in sand subjected to lateral cyclic loads ", *in Proceedings of the 7th International Conference on Physical Modelling in Geotechnics (ICPMG)*. (2010).
40. Kallehave, D. Thilsted, C.L. and Liingaard, M. "Modification of the API py formulation of initial stiffness of sand", *in Offshore Site Investigation and Geotechnics: Integrated Technologies-Present and Future*. Society of Underwater Technology (2012).
41. Abadie, C.N. Byrne, B.W. and Houlsby, G.T. "Rigid pile response to cyclic lateral loading: laboratory tests", *Géotechnique*. **69**(10), pp. 863-876 (2019).
42. Mühlhaus, H.-B. and Vardoulakis, I. "The thickness of shear bands in granular materials", *Geotechnique*. **37**(3), pp. 271-283 (1987).
43. Ovesen, N. "The scaling law relationships, design parameters in geotechnical engineering", *7th ECSMFE, Brighton*. **4**, pp. 319-323 (1979).
44. Chen, R.-p. Sun, Y.-x. Zhu, B., et al. "Lateral cyclic pile-soil interaction studies on a rigid model monopile", *Proceedings of the Institution of Civil Engineers-Geotechnical Engineering*. **168**(2), pp. 120-130 (2015).
45. Yu, G. Gong, W. Chen, M., et al. "Prediction and analysis of behaviour of laterally loaded single piles in improved gravel soil", *International Journal of Civil Engineering*. **17**(6), pp. 809-822 (2019).
46. Walz, B. "Der 1g-Modellversuch in der Bodenmechanik-Verfahren und Anwendung", *Vortrag zum*. **2**, pp. 13-26 (2006).
47. Hettler, A. "Verschiebungen starrer und elastischer Gründungskörper in Sand bei monotoner und zyklischer Belastung", (1981).
48. Little, R.L. and Briaud, J.-L. "Full scale cyclic lateral load tests on six single piles in sand", *Texas A and M Univ College Station Dept of Civil Engineering*, (1988).
49. Lin, S.-S. and Liao, J.-C. "Permanent strains of piles in sand due to cyclic lateral loads", *Journal of Geotechnical and Geoenvironmental Engineering*. **125**(9), pp. 798-802 (1999).

50. Bouafia, A. "Experimental study of repetitive cyclic lateral loading on sand piles using a centrifuge", *in International Journal of Rock Mechanics and Mining Sciences and Geomechanics Abstracts*. (1995).
51. Hadjadji T, F.R.a.D.E. "Analyse du Comportement Expe´rimental de Pieux sous Chargements Horizontaux", *LCPC, Collection Etudes et Recherches, GT74 (in French)*, (2002).
52. Verdure, L. Garnier, J. and Levacher, D. "Lateral cyclic loading of single piles in sand", *International journal of physical modelling in geotechnics*. **3**(3), pp. 17-28 (2003).
53. MHJ, R. "Behavior of Piles and Pile Groups Under Lateral Cyclic Loading," PhD, Ecole Nation des Ponts et Chausse´es, Paris, France, (2009).
54. Li, W. Igoe, D. and Gavin, K. "Field tests to investigate the cyclic response of monopiles in sand", *Proceedings of the Institution of Civil Engineers-Geotechnical Engineering*. **168**(5), pp. 407-421 (2015).
55. Little, R. and Briaud, J. "Cyclic Horizontal Load Tests on 6 Piles in Sands at Houston Ship Channel", *Research Report 5640 to USAE Waterways Experiment Station, Civil Engineering, Texas A&M University*, (1988).
56. Long, J. and Vanneste, G. "Effects of cyclic lateral loads on piles in sand", *Journal of Geotechnical Engineering*. **120**(1), pp. 225-244 (1994).
57. Grabe, J. and Dührkop, J. "Zum Tragverhalten von überwiegend horizontal belasteten Pfählen", *Proceedings of the DGGT Baugrundtagung*. (2008).
58. Cheng, X. Diambra, A. Ibraim, E., et al. "3D FE-informed laboratory soil testing for the design of offshore wind turbine monopiles", *Journal of Marine Science and Engineering*. **9**(1), pp. 101 (2021).
59. Taborda, D. Potts, D. and Zdravković, L. "On the assessment of energy dissipated through hysteresis in finite element analysis", *Computers and Geotechnics*. **71**, pp. 180-194 (2016).
60. Byrne, B.W. "Investigations of suction caissons in dense sand," PhD thesis, University of Oxford, (2000).
61. Abadie, C.N. "Cyclic lateral loading of monopile foundations in cohesionless soils," University of Oxford, (2015).
62. Abongo, K.O. "Model Study of the Static and Cyclic Lateral Capacity of Finned Piles," Lehigh University, (2019).

Figure 1. Modes of soil behavior under cyclic loading

Figure 2. Cyclic response of a laterally loaded pile

Figure 3. Grain size distribution of Firoozkooh sand used in the experiments

Figure 4. Schematic diagram of the test model

Figure 5. Normalized horizontal displacement of the pile with 400 mm embedded length subjected to cyclic lateral loading

Figure 6. Normalized horizontal displacement of the pile with 600 mm embedded length subjected to cyclic lateral loading

Table 10. The "*b*" and "*a*" values from the experimental results

Table 11. Range of "*b*" and "*a*" values from the experimental results

Table 12. Dimension constant (A_H) from the experimental tests

Table 13. Classified values of the dimensionless constant (A_H)

Table 14. The "m_A" and "m_d" values from the experimental results

Table 15. Range of "A_r" and "D_{a0}" from the test results

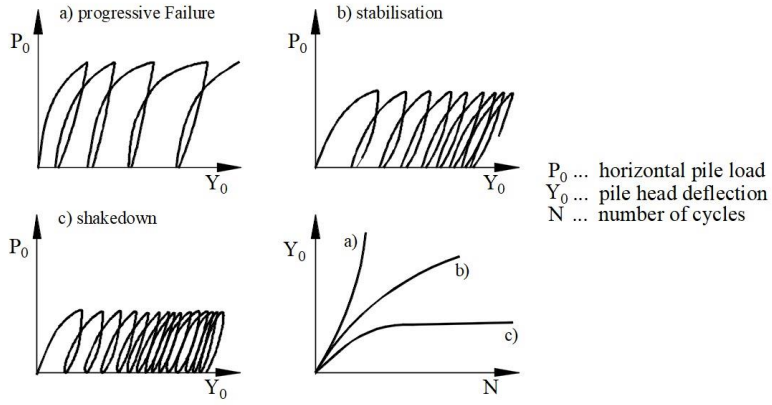

Figure 1. Modes of soil behavior under cyclic loading [7]

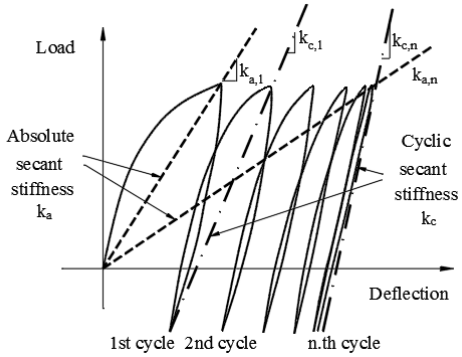

Figure 2. Cyclic response of a laterally loaded pile [16]

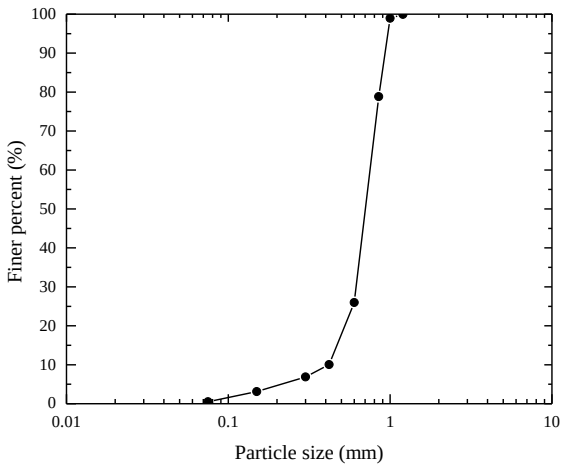

Figure 3. Grain size distribution of Firoozkooh sand used in the

experiments

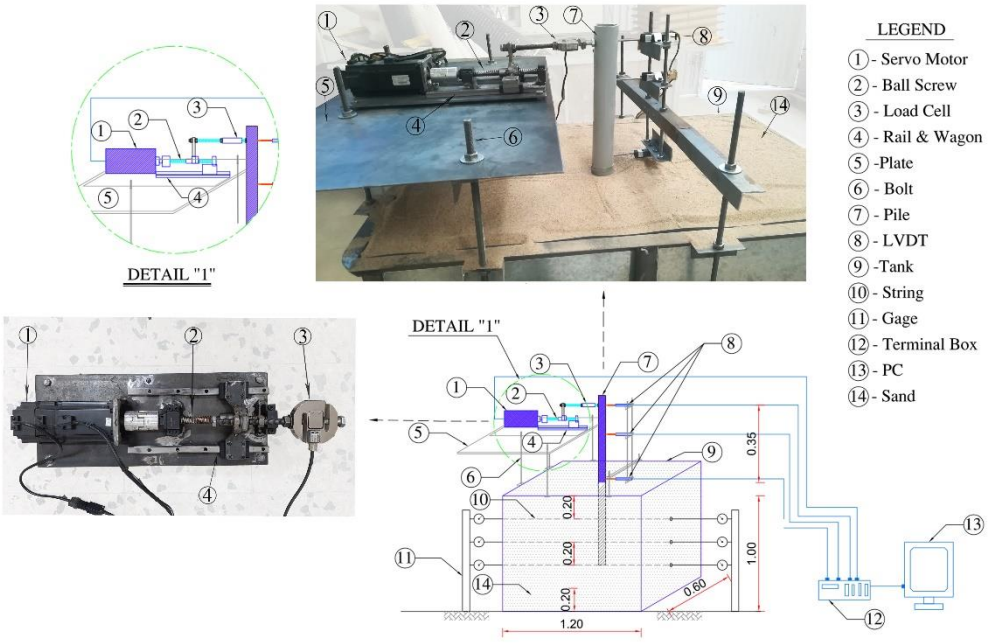

Figure 4. Schematic diagram of the test model

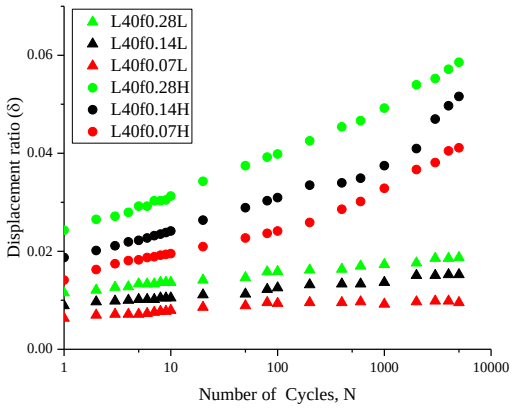

Figure 5. Normalized horizontal displacement of the pile with 400 mm embedded length subjected to cyclic lateral loading

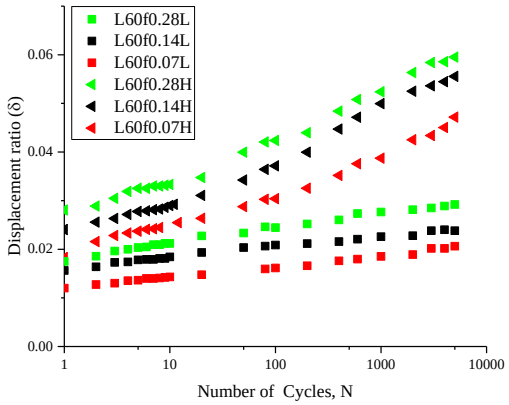

Figure 6. Normalized horizontal displacement of the pile with 600 mm embedded length subjected to cyclic lateral loading

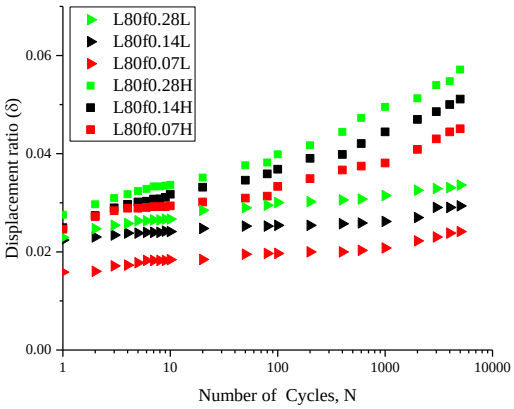

Figure 7. Normalized horizontal displacement of the pile with 800 mm embedded length subjected to cyclic lateral loading

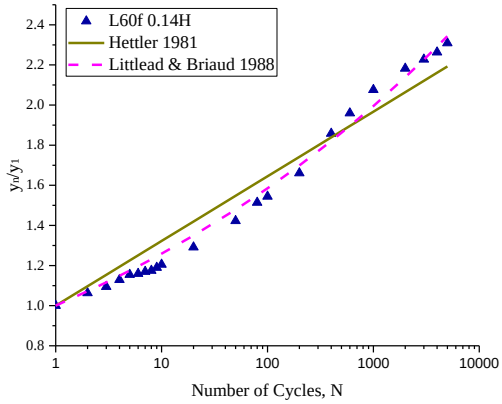

Figure 8. Horizontal displacement of the pile with 600 mm embedded length with logarithmic and power functions

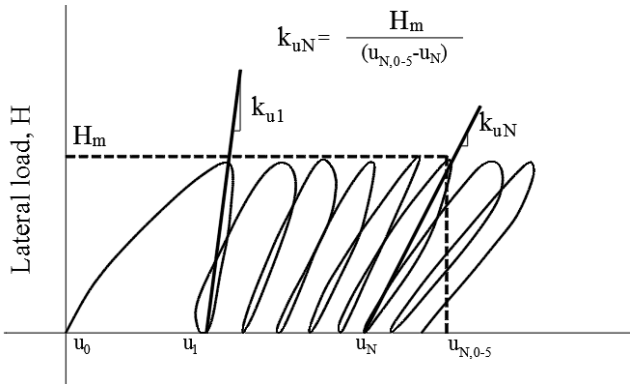

Figure 9. Definition of unloading stiffness

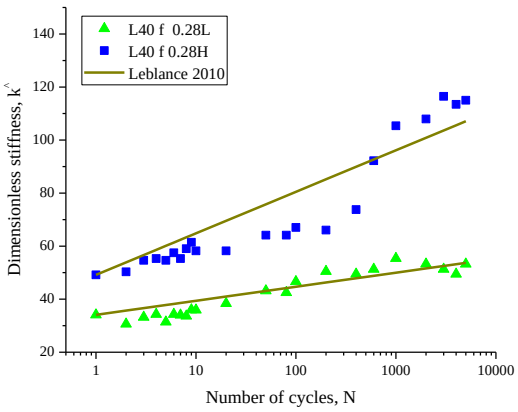

Figure 10. Results of the pile with 400 mm embedded length and 0.28 Hz loading frequency

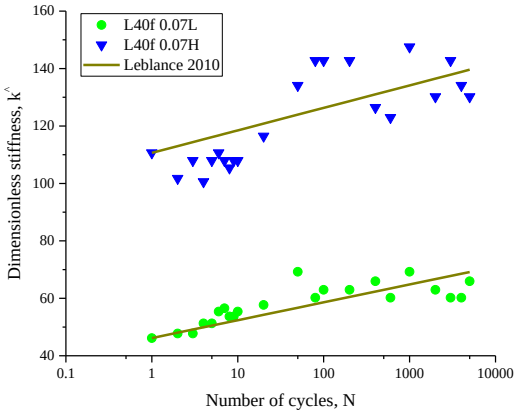

Figure 11. Results of the pile with 400 mm embedded length and 0.07 Hz loading frequency

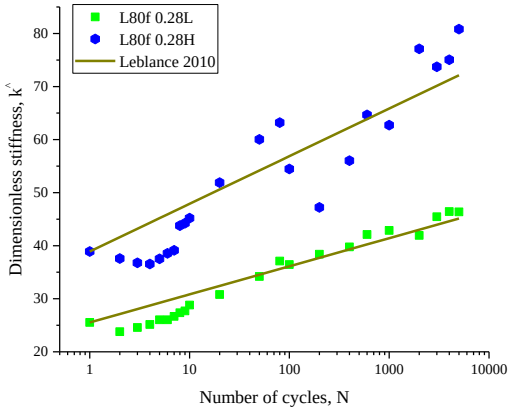

Figure 12. Results of the pile with 800 mm embedded length and 0.28 Hz loading frequency

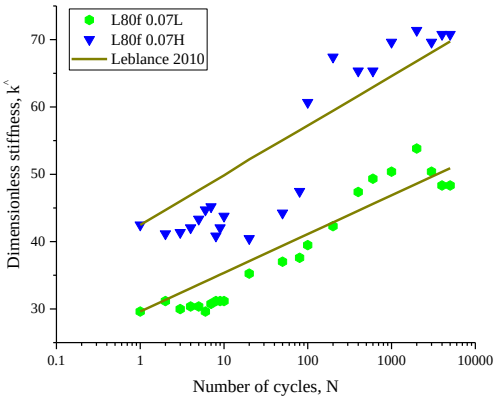

Figure 13. Results of the pile with 800 mm embedded length and 0.07 Hz loading frequency

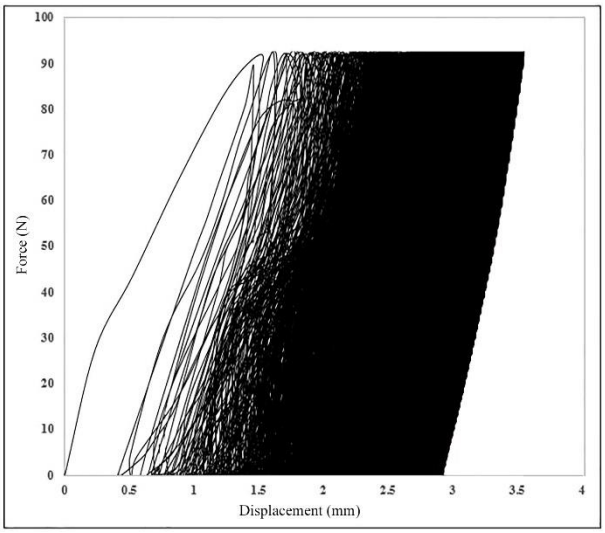

Figure 14. The load-displacement curve of L60f0.14H

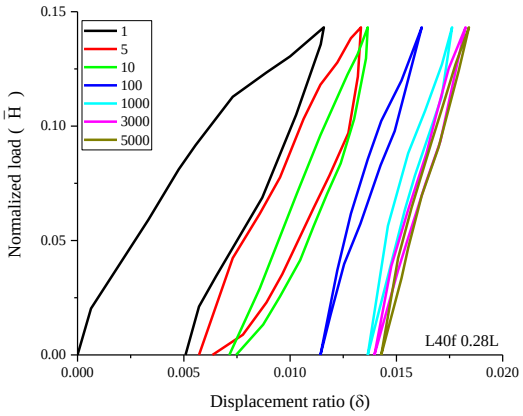

Figure 15. Normalized lateral load and horizontal displacement relationship at various cycles for L40f0.28L

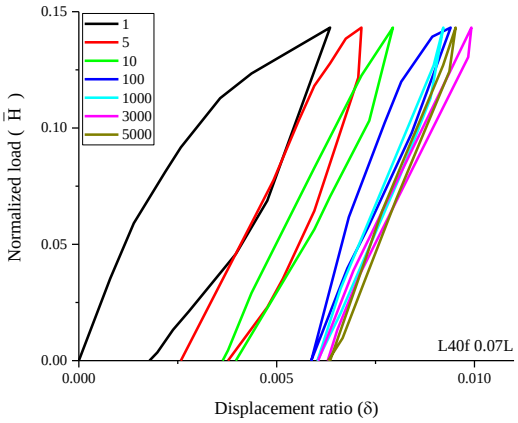

Figure 16. Normalized lateral load and horizontal displacement relationship at various cycles for L40f0.07L

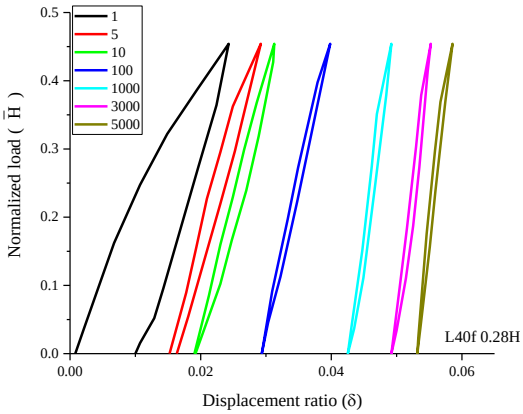

Figure 17. Normalized lateral load and horizontal displacement relationship at various cycles for L40f0.28H

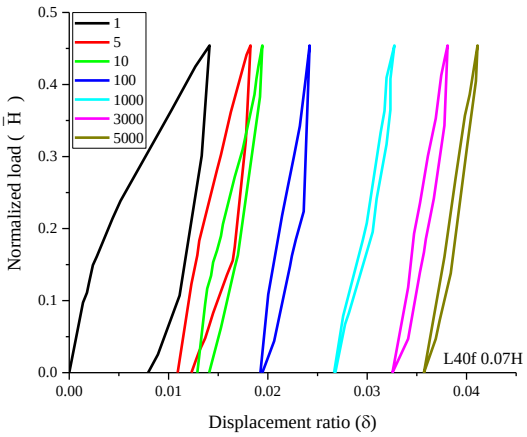

Figure 18. Normalized lateral and horizontal displacement relationship at various cycles for L40f0.07H

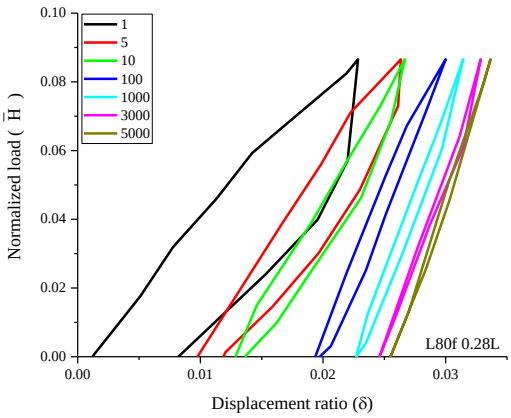

Figure 19. Normalized lateral load and horizontal displacement relationship at various cycles for L80f0.28L

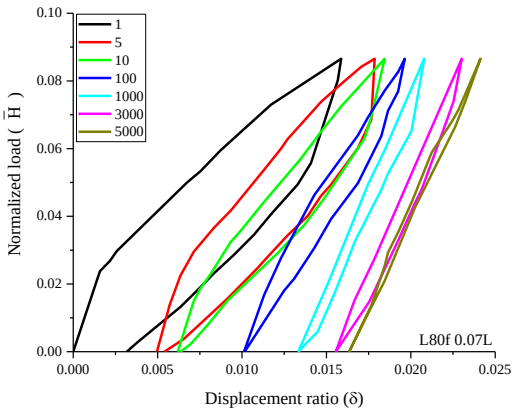

Figure 20. Normalized lateral load and horizontal displacement relationship at various cycles for L80f0.07L

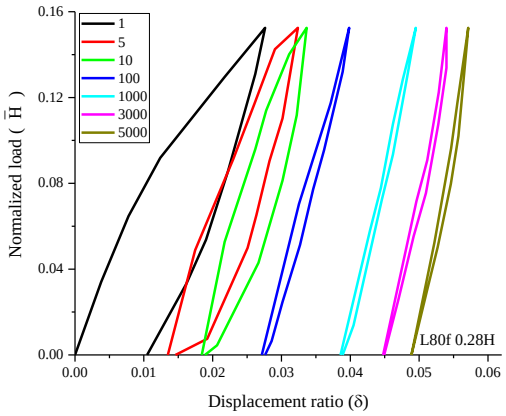

Figure 21. Normalized lateral load and horizontal displacement relationship at various cycles for L80f0.28H

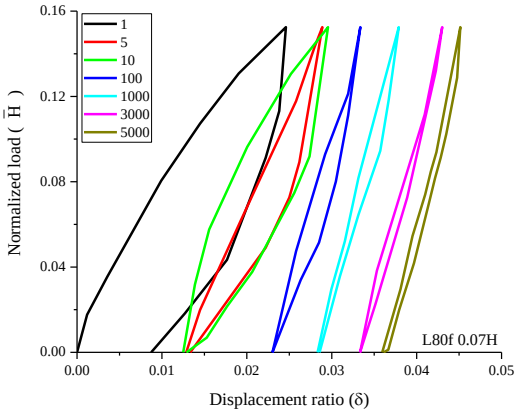

Figure 22. Normalized lateral load and horizontal displacement relationship at various cycles for L80f0.07H

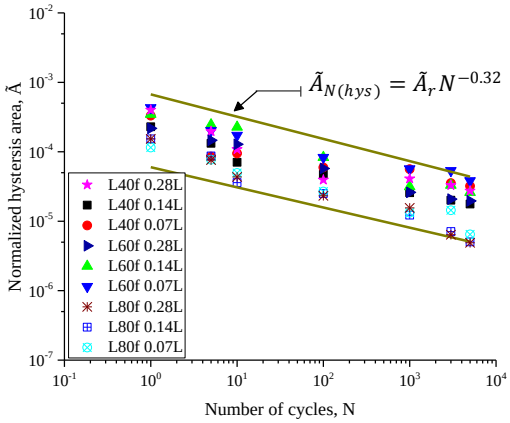

Figure 23. Normalized hysteresis loop area versus number of cycles for loose sand

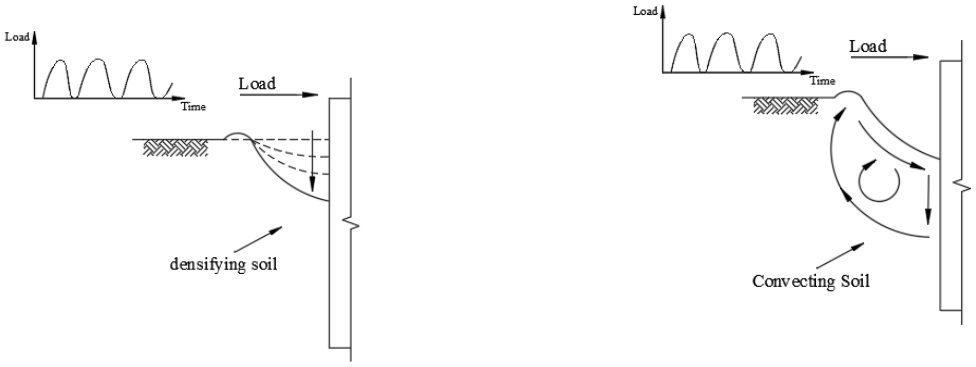

Figure 24. Two phases of densification and convection for a cyclic laterally loaded offshore pile [16]

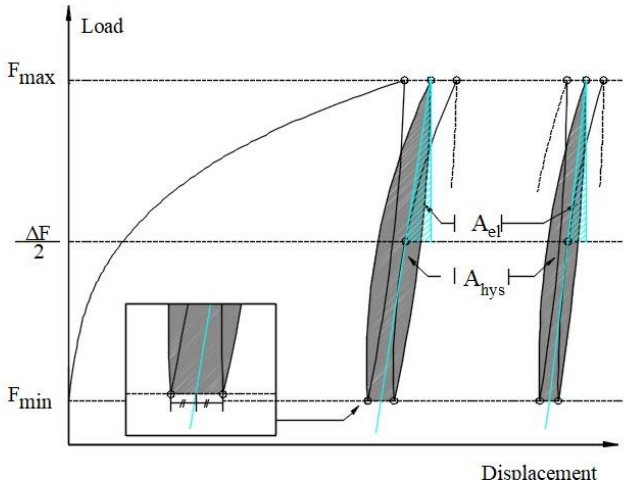

Figure 25. Definition of the cyclic damping ratio [41]

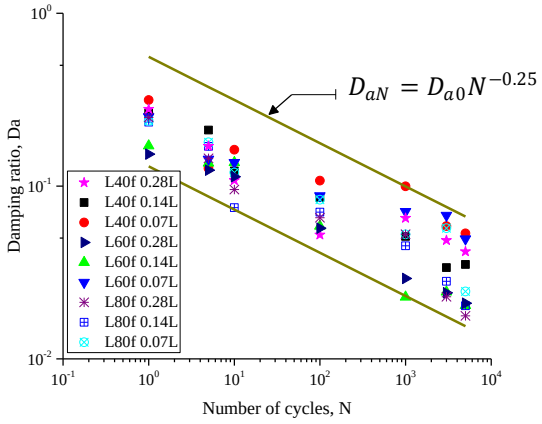

Figure 26. Evolution of the cyclic damping ratio for loose sand

Table 1. Specifications of Firoozkooh sand

Specific gravity, G_s	Average grain size, d_{50}: mm	Uniformity coefficient, C_u	Curvature coefficient, C_c
2.71	0.70	1.8	1.2

Table 2. Properties of the PVC pipe

Weight (N/m)	*EI* (kN.m^2)	Thickness (mm)	Outer diameter (*B*) (mm)
8.6	0.680	2.63	63

EI = stiffness of the pile

Table 3. Strength parameters of Firoozkooh sand

Unit weight, γ_S (kN/m^3)	Relative density, D_r (%)	φ (degree)	E_s (MPa)
13.4	24±1	33	16.4
15.6	97±1	41.5	40

φ = friction angle for the sand; E_s = Young's modulus of the soil

Table 4. Test program

No.	L (m)	f (Hz)	H_{max} (N)	D_r (%)	ξ_b	N
L40f0.28H	0.4	0.28	68.67	97	0.4	5000
L40f0.14H	0.4	0.14	68.67	97	0.4	5000
L40f0.07H	0.4	0.07	68.67	97	0.4	5000
L60f0.28H	0.6	0.28	92.21	97	0.4	5000
L60f0.14H	0.6	0.14	92.21	97	0.4	5000
L60f0.07H	0.6	0.07	92.21	97	0.4	5000
L80f0.28H	0.8	0.28	92.21	97	0.4	5000
L80f0.14H	0.8	0.14	92.21	97	0.4	5000
L80f0.07H	0.8	0.07	92.21	97	0.4	5000
L40f0.28L	0.4	0.28	19.91	24	0.4	5000
L40f0.14L	0.4	0.14	19.91	24	0.4	5000
L40f0.07L	0.4	0.07	19.91	24	0.4	5000
L60f0.28L	0.6	0.28	47.87	24	0.4	5000
L60f0.14L	0.6	0.14	47.87	24	0.4	5000
L60f0.07L	0.6	0.07	47.87	24	0.4	5000
L80f0.28L	0.8	0.28	48.17	24	0.4	5000
L80f0.14L	0.8	0.14	48.17	24	0.4	5000
L80f0.07L	0.8	0.07	48.17	24	0.4	5000
L40H	0.4	Monotonic	-	97	Monotonic	-
L60H	0.6	Monotonic	-	97	Monotonic	-
L80H	0.8	Monotonic	-	97	Monotonic	-
L40L	0.4	Monotonic	-	24	Monotonic	-
L60L	0.6	Monotonic	-	24	Monotonic	-
L80L	0.8	Monotonic	-	24	Monotonic	-

Table 5. Non-dimensional parameters [11]

Horizontal load	$\overline{H} = H / B L^2 \gamma$
Aspect ratio	$\lambda = L / B$
Displacement ratio	$\delta = y / B$

Table 6. Scaling laws for model tests under 1-g conditions [16, 46]

Parameters	Scaling law	Dimension
Length, L	$1/n$	L [m]
Force, H	$1/n^3$	F [N]
Unit weight, γ	1	F/L^3 [N / m^3]
Bending stiffness, EI	$1/n^5$	F * L^2 [N.m^2]
Frequency, f	$n^{1/2}$	1/T [Hz]

n is scaling factor

Table 7. Magnitudes of parameters in prototype and model scale

Parameters		Model scale	Prototype scale
Pile	B(m)	0.063	3.8
	L(m)	0.4, 0.6, 0.8	24, 36, 48
	EI (N.m^2)	$6.8*10^2$	$5.0*10^{11}$
Soil	d_{50} (mm)	0.7	0.7
	γ (kN/m^3)	13.8, 15	13.8, 15
Loads	H (N)	0 ~ 90	0 ~ $1.9*10^7$
	e (m)	0.35	21
	f (Hz)	0.05 ~ 0.3	0.01 ~ 0.04

Table 8. The magnitudes of b proposed by others

Type of test	Soil	Piles	N max	b	Reference
1g model	Dry sand	Stiff	10000	0.2	[47]
Centrifuge	Dry sand	Stiff	5	0.18-0.25	[50]
In situ	Sand	Flexible	100	0.02-0.24	[49]
In situ	Clay & sand	Flexible	10000	0.087	[51]
Centrifuge	Dense dry sand	Flexible	50	0.4-0.18	[52]
Centrifuge	Dry sand	Flexible	500	0.12	[53]
Centrifuge	Dense dry sand	Stiff	1000	0.17-0.25	[20]
1g model	Dry sand	Flexible	10000	0.21	[39]
In situ	Dense sand	Stiff	5000	0.125	[54]

Table 9. The magnitudes of a proposed by others

Type of test	Soil	Piles	N max	a	Reference
In situ	Loose, medium	Flexible	40	0.062-0.086	[55]
1g model	Dense, medium	Flexible	10000	0.12	[39]
In situ	Dense	Stiff	5000	0.085	[54]

Table 10. The "*b*" and "*a*" values from the experimental results

No.	*L*(m)	*b*	$R^2_{(b)}$	*a*	$R^2_{(a)}$	observed
L40f0.28H	0.4	0.15	0.981	0.11	0.975	Stiff
L40f0.14H		0.17	0.923	0.11	0.974	Stiff
L40f0.07H		0.20	0.951	0.12	0.982	Stiff
L60f0.28H	0.6	0.13	0.972	0.09	0.974	Flexible
L60f0.14H		0.14	0.952	0.10	0.990	Flexible
L60f0.07H		0.17	0.978	0.11	0.980	Flexible
L80f0.28H	0.8	0.11	0.973	0.08	0.986	Flexible
L80f0.14H		0.11	0.979	0.08	0.971	Flexible
L80f0.07H		0.09	0.951	0.07	0.964	Flexible
L40f0.28L	0.4	0.08	0.792	0.06	0.944	Stiff
L40f0.14L		0.09	0.973	0.06	0.934	Stiff
L40f0.07L		0.08	0.777	0.06	0.675	Stiff
L60f0.28L	0.6	0.09	0.954	0.06	0.906	Stiff
L60f0.14L		0.06	0.947	0.05	0.871	Stiff
L60f0.07L		0.08	0.992	0.06	0.973	Stiff
L80f0.28L	0.8	0.06	0.913	0.05	0.854	Flexible
L80f0.14L		0.03	0.899	0.03	0.896	Flexible
L80f0.07L		0.05	0.906	0.05	0.888	Flexible

Table 11. Range of "*b*" and "*a*" values from the experimental results

Soil	Piles	*N* max	*b*	*a*
Dense dry sand	Stiff	5000	0.15-0.2	0.11-0.12
	Flexible		0.09-0.17	0.07-0.11
Loose dry sand	Stiff		0.06-0.09	0.05-0.06
	Flexible		0.03-0.06	0.03-0.05

Table 12. Dimension constant (A_H) from the experimental tests

No.	L(m)	A_H	R^2
L40f0.28H		6.80	0.835
L40f0.14H	0.4	8.80	0.824
L40f0.07H		3.40	0.562
L60f0.28H		3.70	0.883
L60f0.14H	0.6	3.30	0.823
L60f0.07H		2.20	0.598
L80f0.28H		3.90	0.827
L80f0.14H	0.8	3.80	0.844
L80f0.07H		3.20	0.773
L40f0.28L		2.30	0.830
L40f0.14L	0.4	1.70	0.520
L40f0.07L		2.70	0.550
L60f0.28L		1.50	0.931
L60f0.14L	0.6	1.40	0.917
L60f0.07L		1.90	0.902
L80f0.28L		2.30	0.918
L80f0.14L	0.8	3.30	0.908
L80f0.07L		2.50	0.875

Table 13. Classified values of the dimensionless constant (A_H)

Soil (Relative density)	Load frequency (Hz)	Stiff piles	Flexible piles
Loose (24%)	0.28	2.3, 1.5	2.3
	0.14	1.4, 1.7	3.3
	0.07	2.7, 1.9	2.5
Dense (97%)	0.28	6.8	3.7, 3.9
	0.14	8.8	3.3, 3.8
	0.07	3.4	2.2, 3.2

Table 14. The "m_A" and "m_d" values from the experimental results

No.	m_A	m_d	No.	m_A	m_d
L40f.28H	0.24	0.10	L40f.28L	0.29	0.20
L40f.14H	0.21	0.11	L40f.14L	0.29	0.25
L40f.07H	0.26	0.21	L40f.07L	0.21	0.17
L60f.28H	0.29	0.19	L60f.28L	0.30	0.24
L60f.14H	0.27	0.19	L60f.14L	0.29	0.25
L60f.07H	0.26	0.20	L60f.07L	0.19	0.15
L80f.28H	0.35	0.24	L80f.28L	0.36	0.28
L80f.14H	0.34	0.24	L80f.14L	0.37	0.26
L80f.07H	0.34	0.25	L80f.07L	0.30	0.22
Average	0.28	0.19	Average	0.32	0.25

Table 15. Range of "A_r" and "D_{a0}" from the test results

Soil (density)	A_r		D_{a0}	
	Min	Max	Min	Max
Dense (97%)	1.20E-04	2.40E-03	0.090	0.445
Loose (24%)	6.00E-05	6.70E-04	0.130	0.560

Brief biographies of authors

First author: Javad Keshavarz

Javad Keshavarz graduated in civil engineering from the Ferdowsi University of Mashhad in 2010. Distinguished as a prominent bachelor's student; he was granted a Master of Science scholarship at the Ferdowsi University in Mashhad and received her master's degree in geotechnical engineering in 2012. Currently, he is studying PhD in the geotechnical field in the department of engineering at the Ferdowsi University of Mashhad. His thesis is about the cyclic behavior of piles subjected to lateral loading.

He has several years of experience as a consultant engineer working on dams and geotechnical tests. He is interested in piles, earth and concrete dams, instrumentation in dams, retaining walls, and the durability of concrete. He has also published some articles in these fields.

Second author: Dr. Jafar Bolouri Bazaz

Jafar Bolouri Bazaz, born in 1958, received BSc (Civil Engineering) from the University of Tabriz in 1984 and an MSc (Structural Eng.) from the University of Tarbiat Modares in 1988. Following four years of practical structural experience in Iran, he did a PhD program on

“Cyclic behavior of granular materials” at the Imperial College of Science & Technology (London, UK) in 1999. Dr Bolouri holds an academic position at Mashhad University as the associate Professor of Geotechnical Engineering. As a geotechnical expert, he has been a supervisor on a number of prestigious projects. During the last two decades, Dr Bolouri has supervised more than 100 MSc and. and 12 PhD students. His publishing includes more than 70 journal papers and 80 conference papers.

Dr Bolouri has 30 years of management, design, construction, and research experience in geotechnical fields (such as dam engineering, problematic soils, soil improvement, and pile and foundation engineering).